Research Article Vol. 9, No. 10 / 1 October 2019 / Optical Materials Express 3895
Optical Materials EXPRESS

Crystal structure, photoluminescence and cathodoluminescence of $Ba_{1-x}Ca_xAl_2O_4$ doped with Eu^{2+}

MAX VOLHARD,[1,2] DANIEL DEN ENGELSEN,[1] GEORGE R. FERN,[1] TERRY G. IRELAND,[1,*] AND JACK SILVER[1,*]

[1] *Centre for Phosphor and Display Materials, Wolfson Centre for Materials Processing, Brunel University London, Uxbridge, Middlesex, UB8 3PH, UK*
[2] *On leave from Department of Chemical Engineering, Münster University of Applied Sciences, Stegerwaldstrasse, 39, Steinfurt, D-48565, Germany*
[*] *jack.silver@brunel.ac.uk*

Abstract: The synthesis, crystal structure, photoluminescence (PL) and cathodoluminescence (CL) spectra of $Ba_{1-x}Ca_xAl_2O_4$ doped with 3 mol% Eu^{2+} between x = 0 and x = 1 are described. The molar fractions of the alkaline earth elements were varied in steps of 0.1. The materials have been synthesized by all solid state reactions at 1300°C in mixed gas (H_2/N_2). The identification of the crystal phases in the samples was based on analyses of the X-ray diffraction patterns. The $Ba_{1-x}Ca_xAl_2O_4$ system contains one dominant monoclinic phase, one dominant hexagonal phase and two different cubic phases that were present in low concentrations. The main characteristic of the PL spectra was that the intensity of the Eu^{2+} photoluminescence decreased upon adding a second alkaline earth ion in the aluminate lattice. The hexagonal and monoclinic phases in the $Ba_{1-x}Ca_xAl_2O_4$ samples showed an unexpected behaviour, namely increasing their unit cell volumes upon decreasing the mole fraction of Ba^{2+}. For the hexagonal phase this behaviour has been explained qualitatively in terms of enhanced spontaneous polarization of the uncompensated anti-ferroelectric state.

1. Introduction

This article is the third part of a study of alkaline earth (Ca, Sr or Ba) aluminates doped with Eu^{2+}. In the first parts [1,2] we have described the crystal structure, photoluminescence (PL) and cathodoluminescence (CL) spectra of $Sr_{1-x}Ca_xAl_2O_4$ and $Sr_{1-x}Ba_xAl_2O_4$ respectively; herein we shall describe the phosphor system $Ba_{1-x}Ca_xAl_2O_4$ doped with 3 mol% Eu^{2+}. For the introduction on the luminescence of alkaline earth aluminates doped with Eu^{2+} we refer the reader to [1] and the literature mentioned therein.

Figure 1 presents the composition diagram of the ternary system BaO-CaO-Al_2O_3, based on the data presented in Shuklás thesis [3], the literature mentioned therein and the work of Ptáček [4] and Ropp [5]. In Fig. 1 the notation of the cement chemistry has been adopted, in which A stands for Al_2O_3, B stands for BaO, and C stands for CaO. These abbreviations will also be used in this paper. The red line BA-CA indicates the compositions that were investigated and are described herein. The compounds in Fig. 1 emphasized with a red mark that are not positioned on the red line could be present as a byproduct of the all-solid state reactions, carried out in the this investigation. The stable compounds in the vicinity of the line BA-CA in Fig. 1 at 1300°C are: CA_2 (calcium di-aluminate or grossite), $C_{12}A_7$ (mayenite) and BC_2A_4 (barium di-calcium tetra-aluminate) and slightly further from the line we have B_3CA (tri-barium calcium aluminate), B_3A (tri-barium aluminate) and C_3A (tri-calcium aluminate). The stability areas of the various

#369384 https://doi.org/10.1364/OME.9.003895
Journal © 2019 Received 10 Jun 2019; revised 22 Aug 2019; accepted 22 Aug 2019; published 3 Sep 2019

Optical Materials EXPRESS

phases in the ternary system of BCA depend critically on the firing temperature. BA has the hexagonal crystal structure (space group $P6_3$); it converts into the more symmetrical hexagonal phase (space group $P6_322$) between 130°C and 170°C. This latter phase is paraelectric while the room temperature phase is ferroelectric [6–8].

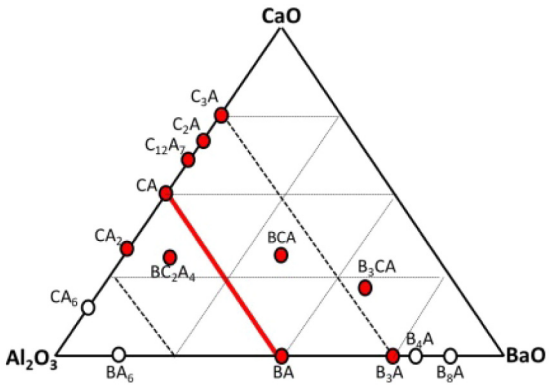

Fig. 1. Composition diagram of BaO-CaO-Al_2O_3. The cement chemistry notation has been adopted to denote the compounds in this ternary system. The red line indicates the compositions that were studied.

Ju et al. [9] studied $Ba_{1-x}Ca_xAl_2O_4:Eu^{2+}$ using cathodoluminescence (CL) and X-ray diffraction (XRD). For $0 < x < 0.15$ they observed two broad bands in the CL spectra, one at about 430 nm and the second at about 500 nm. They also found that the lattice constant for the hexagonal phase at $0 < x < 0.4$ decreased upon increasing the Ca concentration and increased at $x > 0.4$. They assumed that this behaviour was due to the limited solubility of $CaAl_2O_4$ in the $BaAl_2O_4$ host material.

Due to the scarcity of literature on the structure and luminescent properties of BCA doped with a rare earth element, we decided to investigate BCA doped with Eu^{2+} and we shall report the results of this study herein.

2. Experimental

Starting materials for the syntheses were: barium carbonate (Alfa Aesar, UK, 99%), calcium carbonate (Sigma Aldrich, UK, 99.9%), aluminum oxide (SASOL Inc., USA), europium oxide (Ampere Industrie, France, 99.99%), and concentrated hydrochloric acid (Sigma Aldrich, UK, 37%). All materials were used as supplied without further purification. Standard solid state synthesis methods were used to prepare $Ba_{0.97-x}Eu_{0.03}Ca_xAl_2O_4$ with x varying between 0 and 0.97 in steps of 0.1. The samples were prepared by calcining mixtures of an appropriate molar ratio of $CaCO_3$, $BaCO_3$, γ-Al_2O_3 and $EuCl_3$ powders in a flow of 90% N_2–10% H_2. The concentration of Eu^{2+} is indicated in mole percent relative to the alkaline earth ion(s). After calcination the powders were carefully ground by ball milling (Al_2O_3) for 3 hours. The samples were annealed at 1300°C for 3 hours in H_2/N_2 mixed gas; this rather low temperature was necessary to reduce sintering. The reported synthesis conditions were the result of various optimization experiments. The decision on the firing temperature was made after evaluating electron microscope images and photo luminescence (PL) spectra of samples. The electron microscopes including the Gatan spectrometer for recording CL spectra with the transmission electron microscope (TEM), the XRD-equipment and the spectrometer for PL have been described in [1].

Optical Materials EXPRESS

3. Results and discussion

3.1. Electron microscope

The particle size of the alkaline earth aluminates after the high temperature annealing process was rather large and varied from about 0.5 to 6 µm. Figure 2 presents scanning electron microscope (SEM) images of samples after the final annealing step.

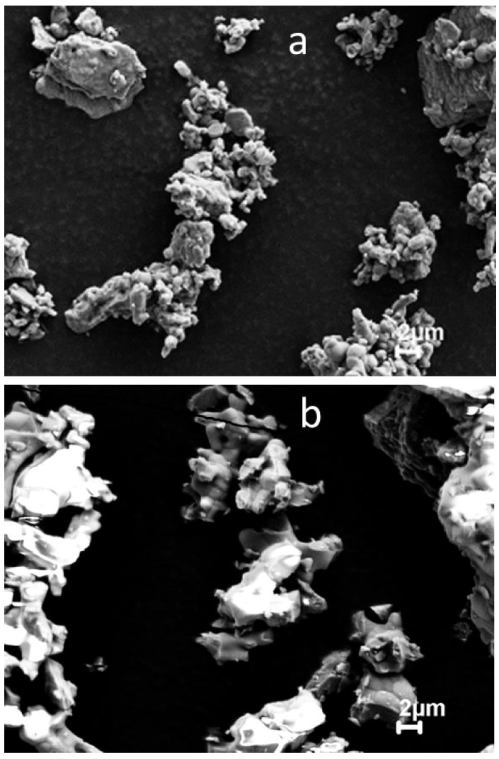

Fig. 2. SEM images of $Ba_{0.97}Eu_{0.03}Al_2O_4$ (a) and $Ba_{0.4}Ca_{0.57}Eu_{0.03}Al_2O_4$ (b) at 7 kV.

Figures 2(a) and 2(b) manifest that crystallites sinter and form agglomerates. At temperatures >1350°C there was more sintering and the agglomerates grew in size. For this reason we have limited the annealing temperatures to 1300°C.

3.2. X-ray diffraction and crystal structure

Figure 3 presents the XRD patterns of $Ba_{0.97-x}Ca_xEu_{0.03}Al_2O_4$ ($0 \le x_{Ca} \le 0.97$).

In BCA doped with Eu^{2+} we have identified 4 different phases as presented in Table 1. The hexagonal BA and monoclinic CA phases occur in large concentrations, while C_3A (tri-calcium aluminate) and $C_{12}A_7$ (mayenite) have much lower concentrations. Fitting was carried out using Bruker's AXS Topas Version 5 using the fundamental parameters fitting method. The phase ratios presented represent the ratio of the crystalline phases present. The parameters of the initial structure for the Rietveld refinement were taken from the various ICDD PDF number standards. The cell parameters of the phases after the refinements have been listed in the Tables 3–6 of the appendix as a function of the Ca mole fraction.

When Table 1 is compared with Fig. 1, it can be seen that of the seven candidate byproducts indicated in Fig. 1 as red dots, we found only C_3A and $C_{12}A_7$. In the BCA series without an Al_2O_3 excess we did not find C_2A (grossite), which was found as a relatively large phase in the

Optical Materials EXPRESS

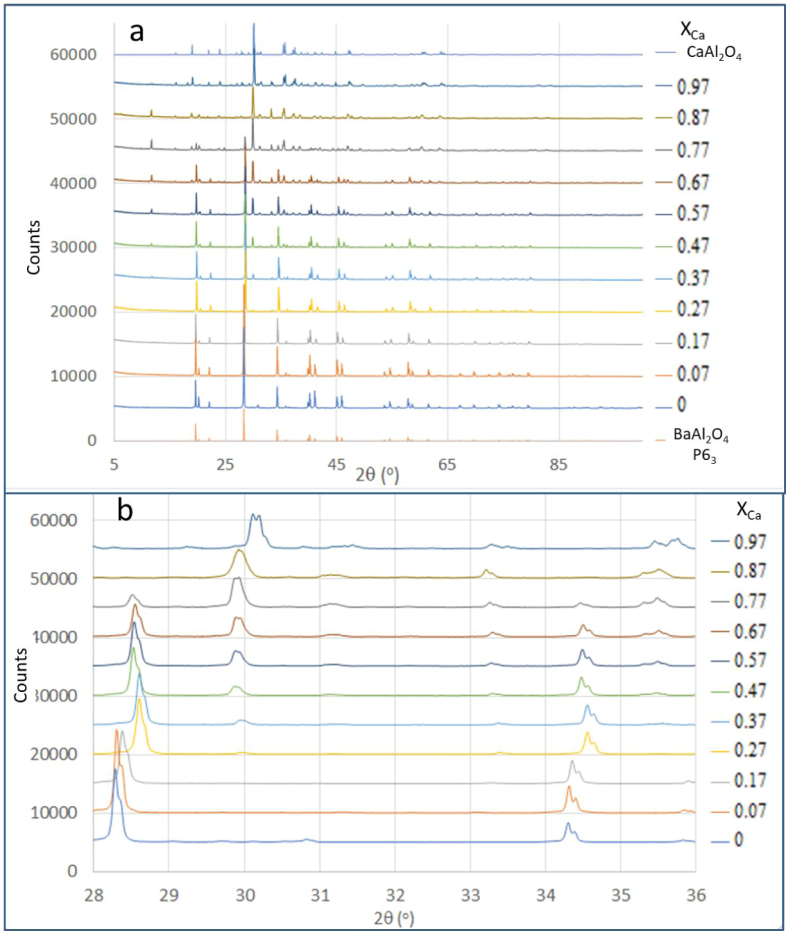

Fig. 3. XRD patterns of $Ba_{0.97-x}Ca_xEu_{0.03}Al_2O_4$ for $0 \le x \le 0.97$. (a) $5° \le 2\theta \le 85°$. (b) Enlarged pattern at $28° \le 2\theta \le 36°$. The $CaAl_2O_4$ and $BaAl_2O_4$ patterns in Fig. 3(a) have been taken from the standard cards ICDD PDF number 01-077-3822 and ICDD PDF number 01-077-4274 respectively.

Table 1. Observed phases in $Ba_{0.97-x}Ca_xEu_{0.03}Al_2O_4$ phosphor series.

Compound	Crystal type	Space group	Table Nr. in appendix	Reference
BA	Hexagonal	$P6_3$	3	6
CA	Monoclinic	$P2_1/n$	4	10
B_3A-C_3A	Cubic	Pm-3m	5	11
$C_{12}A_7$	Cubic	I43d	6	12

system CSA, described in [1]. The cell dimensions of the aluminates with one alkaline earth ion agree well with the data published in the literature [6,10–12].

Figure 4 illustrates the composition of the phases found in BCA doped with Eu^{2+}.

Figure 4 shows that monoclinic BCA based on monoclinic $CaAl_2O_4$ and hexagonal BCA, based on hexagonal $BaAl_2O_4$ are the dominant phases in $Ba_{0.97-x}Ca_xEu_{0.03}Al_2O_4$. In the range $0.2 < x_{Ca} < 0.9$ these phases do not form a solid solution. Ju et al. [9] found that upon annealing BA and CA for 3 days at 1200°C in a H_2S a mixture of hexagonal BCA and monoclinic BCA

Optical Materials EXPRESS

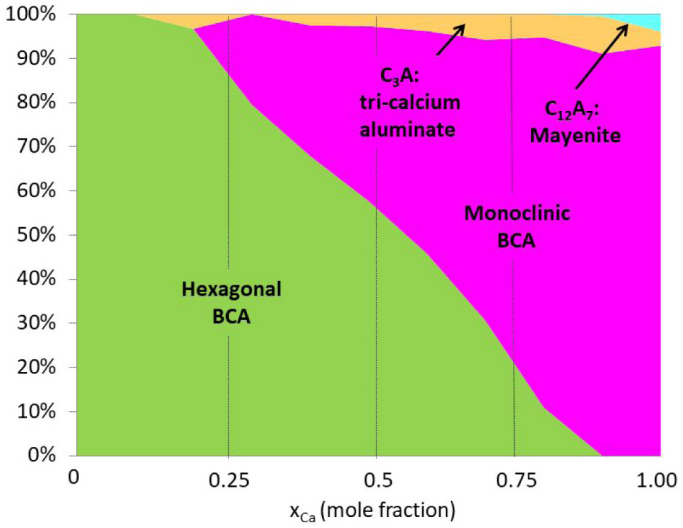

Fig. 4. Composition diagram of the phases in $Ba_{0.97-x}Ca_xEu_{0.03}Al_2O_4$. C_3A is a short notation for $(Ba_{0.97-x}Ca_xEu_{0.03})Al_2O_6$.

phases at $0.2 < x_{Ca} < \approx 0.7$ was obtained. They did not report the presence of C_3A and $C_{12}A_7$ in their samples. It should be noticed that the C_3A and $C_{12}A_7$ phases found in our samples have a deviating stoichiometric ratio $(B_{1-x} + C_x)/A$, which should be 1 after weighing the correct quantities of starting materials. The excess of alkaline earth material in C_3A must be compensated by1-6% Al_2O_3. Since we have not detected alumina lines in the XRD-spectra, we assume that some alumina is present as amorphous material in the samples. This of course means that the presence of C_3A and $C_{12}A_7$ phases leads to Fig. 4 being slightly inaccurate due to the fact that the excess Al_2O_3 (that has not been compensated) has not been included in the phase diagram.

We have described in detail the three sites for the alkaline earth cations in the monoclinic BCA phase (i.e. monoclinic $CaAl_2O_4$ with space group $P2_1/n$) in [1] and also the two sites in hexagonal BSA ($P6_3$) [2]. The paraelectric BA phase ($P6_322$) has only one Ba site; we have used this well-known fact in analyzing the PL spectra, to be discussed in the next section. Figure 5 is a plot of the cell volumes and cell dimensions of the hexagonal and monoclinic phases in the $Ba_{0.97-x}Ca_xEu_{0.03}Al_2O_4$ series. In Fig. 5(b) the cell dimension of the cubic C_3A phase has also been depicted.

The behaviour of the cell volumes of the two largest phases in the $Ba_{0.97-x}Ca_xEu_{0.03}Al_2O_4$ series is surprising and unexpected, because in the range $0.27 < x_{Ca} < 0.77$ the cell volumes increase (Fig. 5(a)) while the Ba-content decreases. Figure 5(b) presents the behaviour of the lattice parameter C of the hexagonal tridymite structure ($P6_322$), which may be considered as the simplest building block of the alkaline earth aluminates [1,6,8,10,13]. For hexagonal BCA with space group $P6_3$ the parameter C is equal to the c-axis as indicated in Table 3, for monoclinic BCA ($P2_1/n$) the lattice parameter C is equal to the a-axis in Table 4 and for the cubic C_3A-B_3A this lattice parameter is equal to the a-axis in Table 5 divided by $\sqrt{3}$. The odd behaviour of the cell volume and lattice parameter C in the range $0.27 < x_{Ca} < 0.77$ has been highlighted by the yellow areas in Figs. 5(a) and 5(b) respectively.

The c-axis of the monoclinic structure jumps at $x_{Ca} = \sim 0.4$ in the reverse direction as the a-axis, shown in Fig. 5(b), which leads to the result that the volume of the monoclinic cell does not change significantly. As mentioned in the introduction, Ju et al. [9] reported a similar effect for the hexagonal phase of BCA; however, they did not provide information on the monoclinic phase. In Fig. 6 the cell volumes of the hexagonal phases in the series

Optical Materials EXPRESS

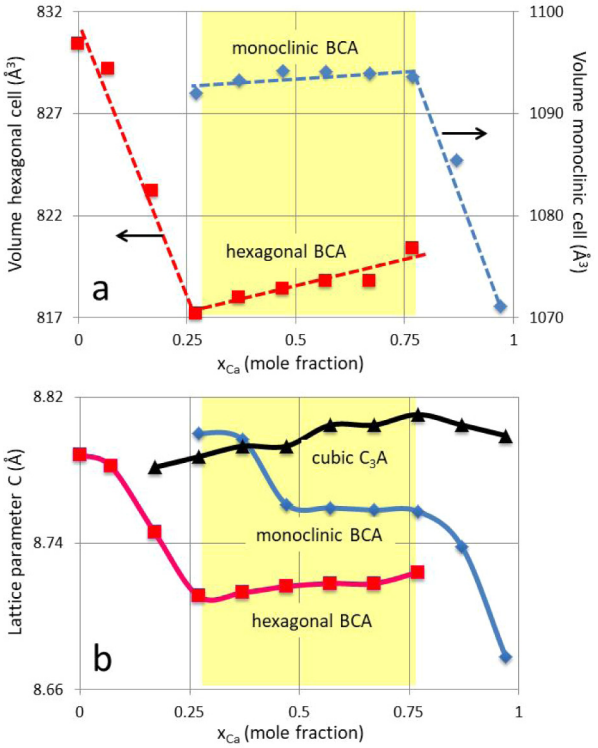

Fig. 5. (a) Cell volumes of hexagonal and monoclinic phases in $Ba_{0.97-x}Ca_xEu_{0.03}Al_2O_4$. (b) Lattice parameter C of hexagonal tridymite structure for the hexagonal, monoclinic and cubic (C_3A) phases in $Ba_{0.97-x}Ca_xEu_{0.03}Al_2O_4$.

$Ba_{0.97-x}Ca_xEu_{0.03}Al_2O_4$, $Sr_{0.97-x}Ba_xEu_{0.03}Al_2O_4$ and $Sr_{0.99-x}Ca_xEu_{0.01}Al_2O_4$ (data taken from [1] and [2]) have been plotted. Even though the space group (or ferroelectric state) of the hexagonal phase in $Sr_{0.99-x}Ca_xEu_{0.01}Al_2O_4$ has not been identified herein, it is assumed that the actual space group does not affect this comparison.

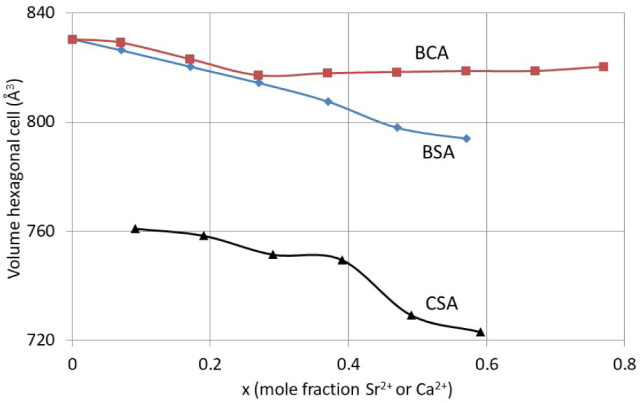

Fig. 6. Volumes of the hexagonal unit cell in $Ba_{0.97-x}Ca_xEu_{0.03}Al_2O_4$ (BCA), $Sr_{0.97-x}Ba_xEu_{0.03}Al_2O_4$ (BSA) and $Sr_{0.99-x}Ca_xEu_{0.01}Al_2O_4$ (CSA).

Optical Materials EXPRESS

The volume of the hexagonal structure in the BCA system shows deviating character as presented in Fig. 5(a) and described above, whereas the volumes of the hexagonal cells in the other aluminate systems (presented in Fig. 6) have a conventional behaviour, viz. decreasing in size upon decreasing the content of the large Ba^{2+} or Sr^{2+} ions. This surprising result is discussed in more detail in section 4 of this article.

3.3. PL and CL spectra

In Figs. 7(a) and 7(b) the PL emission and excitation spectra respectively of the phosphor series BCA have been plotted for various values of the molar fraction of Ca.

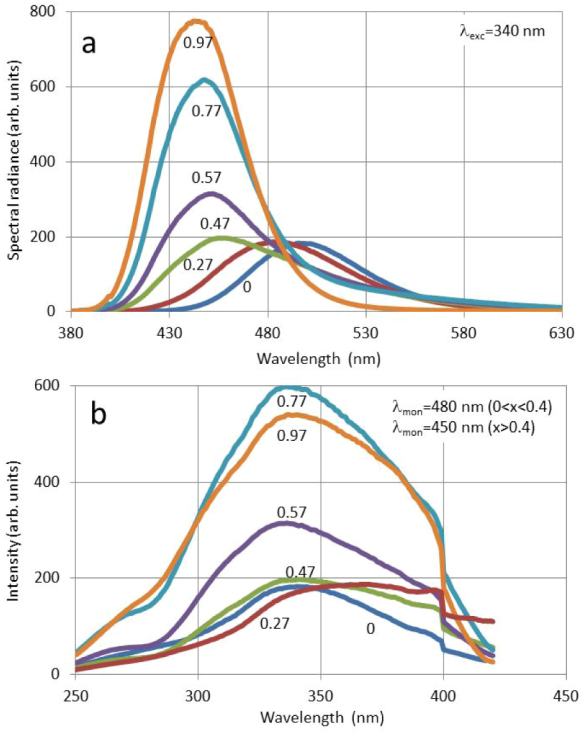

Fig. 7. PL spectra of $Ba_{0.97-x}Ca_xAl_2O_4$:3%Eu^{2+} at various values of x_{Ca}. (a) Emission spectra; for $0.2 < x < 0.4$ the excitation wavelength was 360 nm. (b) Excitation spectra. For clarity reasons only a limited number of spectra are shown. The kink at 400 nm in the excitation spectra is due to a filter change of the spectrometer.

The spectra in Fig. 7(a) feature broadening of the emission band at $0.3 < x_{Ca} < 0.8$. This range corresponds well with the range of x_{Ca} where two different phases were found in sufficiently high concentrations, as indicated in Fig. 4. These two phases have different crystal structures and create different electrostatic environments for the Eu^{2+} ions, which leads to band broadening. Although these two phases correspond with the phases of pure BA and CA, the spectra in Fig. 7a are not identical with the corresponding linear combinations of the spectra of the mother compounds; this can easily be verified from the spectrum of $Ba_{0.5}Ca_{0.47}Eu_{0.03}$ Al_2O_4, which is not the 50/50 linear combination of the spectra of $Ba_{0.97}Eu_{0.03}Al_2O_4$ and $Ca_{0.97}Eu_{0.03}Al_2O_4$.

Ju et al. [9] published the CL-spectra (10 kV excitation) of the BCA series doped with Eu^{2+}. They found deviating spectra for the samples with a high Ba content: instead of only one emission band with $\lambda_0 \approx 500$ nm, they found a second band at about 430 nm. This second emission band seems to be related to the hexagonal structure, because it disappeared between x_{Ca}=0.15 and

Optical Materials EXPRESS

x_{Ca}=0.4. This 430 nm emission band was not detected in our PL spectra of $Ba_{1-x}Ca_xAl_2O_4:Eu^{2+}$ illustrated in Fig. 7(a), nor was it present in the CL spectrum of $BaAl_2O_4:Eu^{2+}$ recorded at 200 keV and room temperature, as indicated in Fig. 9(a) hereafter. The emission spectrum of $CaAl_2O_4:Eu^{2+}$ (x_{Ca}=0.97) in Fig. 7(a) is similar to the PL spectrum measured at 300 K by Ueda et al. [14]. By comparing the PL spectrum of BA (x_{Ca}=0) in Fig. 7(a) with literature data some surprising differences are apparent regarding the presence or absence of a second emission band at 430 nm [9,15–22]. These differences are represented in Table 2 as the ratio R, which is the spectral radiance at 430 nm divided by the spectral radiance at 500 nm. Although this table does not present the results of all publications relating to the emission band of $BaAl_2O_4:Eu^{2+}$, we assume that the key information is displayed.

Table 2. Ratio between spectral radiances at 430 nm and 500 nm of $BaAl_2O_4:Eu^{2+}$

R	Spectrum	Annealing temp. (°C)	Annealing gas	co-dopant	Ref.
1.3	PL	500	combustion gases	Dy^{3+}	17
0.25	PL	550	combustion gases	none	18
0.05-0.5	PL	1500	air	Dy^{3+}	19
0.1	PL	1350	H_2/N_2	Dy^{3+}	20
0.8	CL	1200	H_2/N_2	none	9
n. s. [1])	PL	≈1400	H_2/N_2	none	15
n. s. [1])	PL	1200	H_2/N_2	none	16
n. s. [1])	PL	1400	air/TCRA[2])	none	21
≈0.25	PL	≈1400	H_2/N_2	none	22
2.8	CL[3])	1350	H_2/N_2	none	2
n. s. [1])	PL & CL[4])	1350	H_2/N_2	none	This work

[1]) n. s. is no shoulder or emission band at about 430 nm.
[2]) Thermal carbon reducing atmosphere.
[3]) $Ba_{0.9}Sr_{0.07}Eu_{0.03}Al_2O_4$, measured at −170°C.
[4]) See Fig. 8(b).

It is impossible to indicate one factor that is responsible for the different values of R in Table 2; however, it seems that the combination of adding a co-dopant and annealing at low temperature is maximizing R. It is tempting to compare the 430 nm band observed by various workers in the PL spectrum of $BaAl_2O_4$ with the low temperature 440 nm emission band in $SrAl_2O_4$, because the similarity of the ~435 nm bands in the spectra of $BaAl_2O_4$ and $SrAl_2O_4$ is striking [1]. In our study on $Sr_{1-x}Ca_xAl_2O_4:Eu^{2+}$ we have proposed to assign the 440 nm band in $SrAl_2O_4$ to an F-centre [1]. Support for this assignment was obtained in our study of the BSA series [2], where the 430 nm band in the low temperature CL spectrum of $Ba_{0.9}Sr_{0.07}Eu_{0.03}Al_2O_4$ was found to be much stronger than the 500 nm band. It was outside the scope of the present work to investigate the cause of the differences shown in Table 2. As already mentioned by Peng and Hong [21], more investigations are necessary to clarify this problem. Currently we are investigating the PL and CL of $BaAl_2O_4$, doped with Eu and without any dopant.

In Fig. 8 the deconvolutions of various PL-spectra of the $Ba_{0.97-x}Ca_x\ Eu_{0.03}Al_2O_4$ series are presented.

The fitting of the deconvoluted spectrum to the experimental spectrum was carried out with a minimum set of Gaussian profiles and using a least squares algorithm in a wavenumber (cm^{-1}) representation as described previously [1,23,24]. The spectra of Figs. 8(b), 8(c) and 8(d) can be well represented by two Gaussian profiles whereas the spectrum for $Ca_{0.97}Eu_{0.03}Al_2O_4$ needs three Gaussian profiles. Figure 8(a) has been taken from [1].

Optical Materials EXPRESS

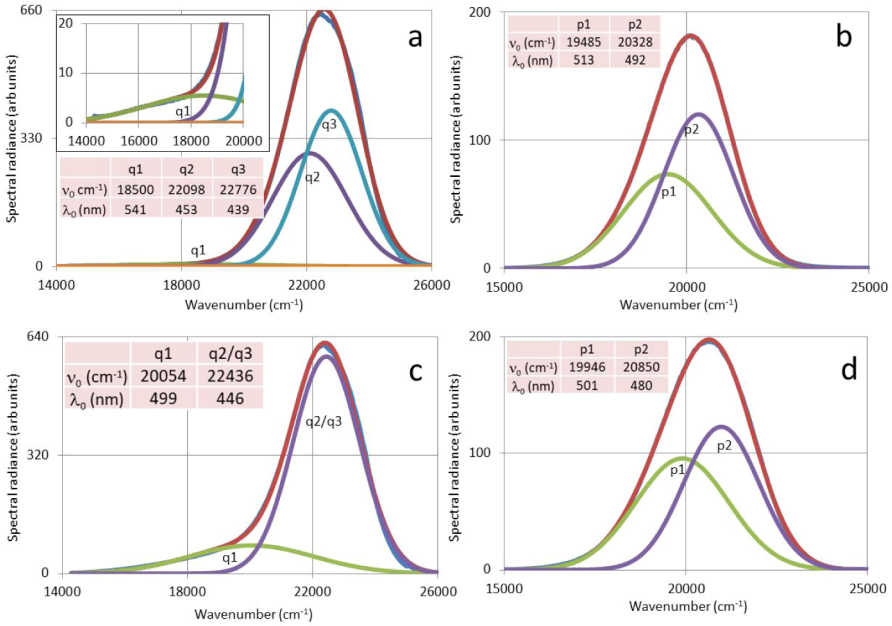

Fig. 8. Deconvolutions of PL spectra of BCA doped with Eu^{2+}. (a) $Ca_{0.97}Eu_{0.03}Al_2O_4$.; the inset shows a part of the spectrum at an enlarged scale (taken from [1]). (b) $Ba_{0.97}Eu_{0.03}Al_2O_4$. (c) $Ba_{0.2}Ca_{0.77}Eu_{0.03}Al_2O_4$. (d) $Ba_{0.7}Ca_{0.27}Eu_{0.03}Al_2O_4$. The p-profiles refer to the hexagonal ($BaAl_2O_4$) phase, whereas the q-profiles refer largely to the monoclinic ($CaAl_2O_4$) phase.

Before discussing the spectra presented in Fig. 8, a short description of the monoclinic BCA phase is helpful. The unit cell of this phase contains 12 Ca/$BaAl_2O_4$ units and has three alkaline earth cation sites, which are labelled Ca(1), Ca(2) and Ca(3), having equal multiplicity. The first two sites are six-coordinated, in which the O^{2-} anions belong to four different AlO_4 tetrahedra [10]. These sites are located in one of the channels formed by the rings made by the AlO_4 tetrahedra. The cation site Ca(3) is different, since it is located in the second channel and it has nine O^{2-} anion nearest neighbours belonging to five different AlO_4 tetrahedra. In our previous work [1] we have assigned the q3 and q2 profiles in Fig. 8a to emission from Eu^{2+} situated at the Ca(3) site. This site is roomy and can easily lodge the Eu^{2+} ion. From the asymmetry of the 440 nm band in Fig. 8a we have concluded that there are two positions for the Eu^{2+} ions at the Ca(3) lattice site [1]. As the radiances of q2 and q3 are almost equal, it is likely that these two Ca(3) sites have equal probabilities of being occupied.

The q1 profile in Fig. 8a is attributed to Eu^{2+} situated at the Ca(2) and Ca(1) sites. By adding 20% Ba, the q1 band grows substantially and experiences a blue shift, while the main band may be represented by a single Gaussian (Fig. 8(c)). We assume that this may be explained by the presence of the hexagonal ($BaAl_2O_4$) phase which has a concentration of 10.9% in the $Ba_{0.2}Ca_{0.77}Eu_{0.03}Al_2O_4$ sample of Fig. 8c

Figures 8(b) and 8(d) refer to the Ba-rich, hexagonal side of the BCA-series, viz. $Ba_{0.97}Eu_{0.03}Al_2O_4$ and $Ba_{0.7}Ca_{0.27}Eu_{0.03}Al_2O_4$. Kawaguchi et al. [25] found that adding a small amount of Sr to $BaAl_2O_4$ gave rise to a phase transition from ferroelectric to paraelectric $BaAl_2O_4$. In the study on the BSA series that we have published recently [2], this could be verified from an analysis of the PL spectra: the spectrum of the $Sr_{0.07}Ba_{0.9}Eu_{0.03}Al_2O_4$ sample could be represented by one single Gaussian profile. This is evidence for a hexagonal phase with only one alkaline earth cation

Optical Materials EXPRESS

site: the more symmetrical paraelectric structure. Herein the spectra of the BCA series with low x_{Ca} were analysed in the same way. It was found that for an appropriate deconvolution, two Gaussian profiles were needed, as indicated in Fig. 8(d). Hence, by adding Ca to $BaAl_2O_4:Eu^{2+}$ the ferroelectric structure of $BaAl_2O_4$ is maintained and does not convert to the paraelectric phase at $0 < x_{Ca} < 0.3$. This is an interesting difference with the BSA series.

Figure 9(a) manifests the CL spectra of a $BaAl_2O_4$:3%Eu^{2+} sample that had been stored for 3 years in air at room temperature. Spectrum 1 refers to a specimen that was not hit by electrons before recording. This CL-spectrum compares favourably with the PL spectrum illustrated in Fig. 8(b) and that of Blasse and Bril [15], while the PL spectrum of $BaAl_2O_4:Eu^{2+}$ recorded at 4.2 K by Poort et al. [16] has a narrower band width and is somewhat red-shifted. After reannealing this three-years-old $BaAl_2O_4$:3%Eu^{2+} sample at 1350°C in H_2/N_2, a CL spectrum was recorded that was identical with spectrum 1 in Fig. 9(a). After about five minutes of electron bombarding the $BaAl_2O_4:Eu^{2+}$ specimen (shelf life sample) at 200 keV in the TEM, the spectrum was recorded again: it had changed drastically (2). It can be seen that there is a lot of Eu^{3+} in the sample: the electron bombardment apparently catalysed the oxidation of Eu^{2+} to Eu^{3+}. Spectra that were recorded of this $BaAl_2O_4:Eu^{2+}$ sample at intermediate times manifested lower intensity Eu^{3+} peaks (with their intensities roughly proportional to the time of electron bombardment) than spectrum 2 in Fig. 9(a). Samples of $SrAl_2O_4:Eu^{2+}$ and $CaAl_2O_4:Eu^{2+}$ that had a shelf life of 3 years in air at room temperature were also examined in these studies; however, these samples were

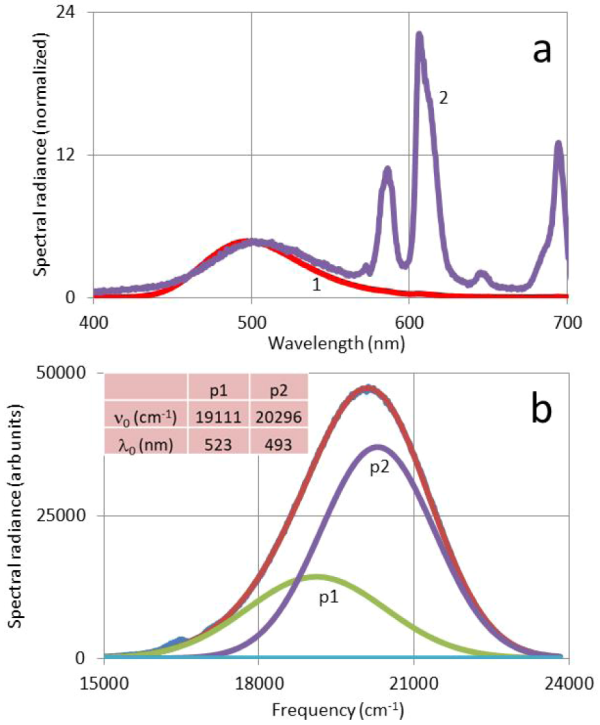

Fig. 9. CL spectra recorded at 200 keV and room temperature of a $BaAl_2O_4$:3%Eu^{2+} sample that has been stored for three years in air at room temperature. (a) The spectral radiance of the spectra has been normalized at λ=500 nm. First spectrum 1 was recorded (without e-beam exposure before recording), spectrum 2 was recorded after about 5 minutes electron bombardment of the same specimen in the TEM. (b) Deconvolution of spectrum 1 (from (a)) with two Gaussian profiles.

Optical Materials EXPRESS

stable upon prolonged electron bombardment and did not show any sign of Eu^{3+}. From these results it is concluded that H_2O and O_2 have diffused into the bulk of $BaAl_2O_4$:Eu^{2+}, because an adsorbed layer of H_2O, O_2 and CO_2 at the surface of the crystals would be insufficient to oxidize sufficient Eu^{2+} to Eu^{3+} to observe the strong Eu^{3+} luminescence in Fig. 9(a). It may thus be concluded that this absorption of oxidizing gases into $SrAl_2O_4$:Eu^{2+} and $CaAl_2O_4$:Eu^{2+} crystals did not occur during the shelf life. Rezende et al. [26] found that the spectrum of $Sr_{1-x}Ba_xAl_2O_4$ (BSA) doped with Eu^{2+} manifested Eu^{3+} characteristics upon irradiation with high energetic X-rays. Since their samples were annealed in air, we assume that some oxygen was absorbed by the crystals and that the same oxidation mechanism played a role in BSA doped with Eu^{2+}.

Figure 9(b) is the deconvolution of spectrum 1 in Fig. 9(a). The result deviates slightly from the deconvolution of the PL spectrum illustrated in Fig. 8(b) and deviates also from the result published by Poort et al. [16]. These authors found p1 and p2 at 540 nm and 510 nm, while here they are found at 523 nm and 493 nm respectively; the band p1 refers to Eu(1) ions (Eu^{2+} ions at Ba site 1) and p2 to Eu(2) ions (Eu^{2+} ions at Ba site 2). This assignment is based on the ratio of the radiances of the two bands: ideally it should be 3 (p2/p1), here it is found to be 2.1, while Poort et al. found that it was about 3. This factor reflects the multiplicity ratio between the numbers of Ba^{2+} ions in the two cation sites of ferroelectric $BaAl_2O_4$. The conclusion of Poort et al. was largely confirmed by Stefani et al. [19], although these latter authors measured the two bands in the PL spectrum of $BaAl_2O_4$:Eu^{2+},Dy^{3+} at λ_0=435 nm and 500 nm Finally, He et al. [20] measured a band at 419 nm in $BaAl_2O_4$:Eu^{2+}. In the PL spectra reported herein bands at 435 nm and 419 nm were not observed. As mentioned above, this scientific debate has not yet been resolved and this issue needs more research.

4. Ferroelectricity of $Ba_{0.97-x}Ca_xAl_2O_4$:3%Eu^{2+}

In this section the surprising results presented in Figs. 5 and 6 are discussed. The surprise is the increase of the cell volumes of both the hexagonal and monoclinic phases in $Ba_{0.97-x}Ca_xAl_2O_4$:3%Eu^{2+} upon increasing the content of Ca, which has a much smaller ion diameter than Ba. The hexagonal structure of $BaAl_2O_4$ in the distorted structure (space group $P6_3$) is illustrated in Fig. 10: the view is parallel to the hexagonal c-axis.

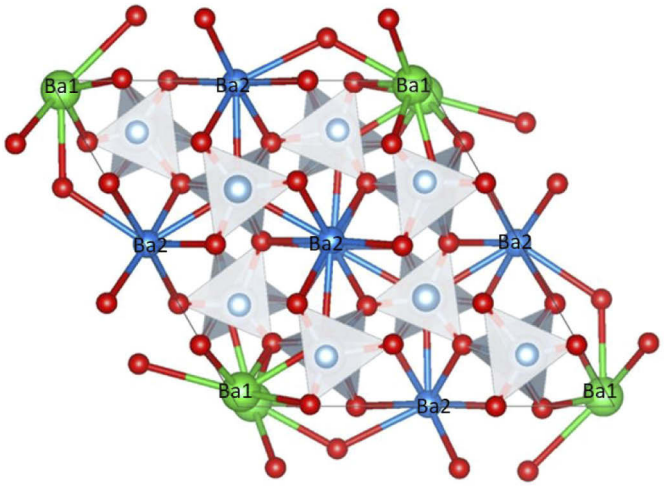

Fig. 10. View of the hexagonal unit cell (space group $P6_3$) of $BaAl_2O_4$ along the c-axis. Ba^{2+} ions at site 1 are indicated by Ba1 (green), Ba^{2+} ions at site 2 are indicated by Ba2 (blue). Red balls are O^{2-} ions and the Al^{3+} ions are indicated inside the tetrahedra.

Optical Materials EXPRESS

The question is: what happens to the structure depicted in Fig. 10 when the large Ba^{2+} ions are replaced by the smaller Ca^{2+} ions? Up to x_{Ca}=0.27 the Ca ions can be inserted without giving rise to critical mechanical tension in the lattice, which results in a gradual decrease of the cell volume, as illustrated in Figs. 5(a) and 5(b). The decrease of the cell dimensions when the Ca molar fraction is increased from 0 to 0.27 is 0.9% for the a-axis and 0.35% for the c-axis, while the decrease of ionic radius in going from Ba^{2+} to Ca^{2+} is 23%. The Ca^{2+} ions are too small for the Ba-cavities: they are "rattling" in these cavities. As described by Huang et al. [7,27], $BaAl_2O_4$ is not a classical ferroelectric material such as $BaTiO_3$, but rather a ferrielectric material with spontaneous antiparallel polarizations in two sub-lattices that do not compensate each other. This explains the rather low values for the spontaneous polarization and the dielectric constant. The displacement of the Ca ion in the Ba-cavity can be much larger in the [001] direction, which may create a much larger polarization. However this much larger displacement of the Ca^{2+} ions can only be stabilized if there are enough Ca^{2+} ions to interact and consequently to lower the free energy of the system [27,28]. It is assumed that Ca^{2+} ions at the Ba(1) site move in one direction and those at the Ba(2) site move in the opposite direction from x_{Ca}=0.27 onwards, then although the resulting polarizations will be antiparallel, they do not compensate each other because of the difference between the numbers of Ba(1) and Ba(2) sites; thus, the total spontaneous polarization is expected to increase. This polarization effect is the driving force to resist further shrinking of the structure as indicated in Figs. 5 and 6. The channels of the AlO_4 tetrahedra in aluminates like BCA determine largely the dimension of the unit cell. This refers mainly to the widths of the channels, which are measured in the a-b plane, perpendicular to the hexagonal axis. What happens in this ferroelectric phase is that the displacements of Ca^{2+} ions in the [001] direction causes strain in the rings of tetrahedra preventing them from contracting upon the introduction more Ca^{2+} ions. This strain is strong enough to slightly inflate the cell dimension from x_{Ca}=0.27 to 0.77. The large anisotropic displacement ellipsoid of the O1 anion in the a-b plane of the $BaAl_2O_4$ lattice reported by Kawaguchi et al. [25] is an important piece of information that supports this hypothesis. Herein this hypothesis on ferroelectricity in hexagonal $Ba_{0.97-x}Ca_xEu_{0.03}Al_2O_4$ has not been tested by measuring the polarization and dielectric constant, as these measurements were outside the scope of the present research: we are planning to investigate the effect(s) of ferroelectricity in these materials in the near future.

The correspondence between the behaviour of the hexagonal and monoclinic phases in Fig. 5 suggests that the mechanisms underlying the odd behaviour is or could be similar for both structures. Figs. 5(a) and 5(b) show that the reverse behaviour in the monoclinic phase is less evident than in the hexagonal phase. Nevertheless, at x_{Ca}<0.77 both volume and lattice parameter C change clearly. Monoclinic $Ba_{0.97-x}Ca_xAl_2O_4$:3%Eu^{2+} has the structure of $CaAl_2O_4$, which does not show ferroelectricity. It is therefore less obvious that the behaviour of the cell volume and cell dimension of monoclinic CA in Fig. 5 can be explained in terms of ferroelectricity. For the monoclinic structure the a-axis is perpendicular to the rings of six AlO_4 tetrahedra that form the skeleton of the crystal structure. In going from $Ca_{0.97}Eu_{0.03}Al_2O_4$ to $Ba_{0.77}Ca_{0.2}Eu_{0.03}Al_2O_4$ the cell volume increases by 2.1%, while the total volume of the alkaline earth ions ($V_{Ca} + V_{Ba}$) increases by 24% for the monoclinic structure. This shows that the monoclinic aluminate structure is rather roomy, because it is able to absorb the bulky Ba ions without large dimensional changes. The Rietveld refinements of the XRD-patterns of the $Ba_{0.97-x}Ca_xAl_2O_4$:3%Eu^{2+} samples showed that at x_{Ca}<0.77 the hexagonal phase has a larger Ba occupancy than the monoclinic phase, which enables the monoclinic phase to largely maintain its dimensions upon further increasing the molar fraction of Ba. In spite of the absence of ferroelectric phases in $CaAl_2O_4$, we cannot exclude ferroelectricity in monoclinic $Ba_{0.97-x}Ca_xEu_{0.03}Al_2O_4$ in the range 0.27 < x_{Ca}<0.77, because the built-in Ba ions have inflated the channels formed by the AlO_4 tetrahedra slightly which creates more space for the Ca^{2+} ions to move and eventually leads to spontaneous polarization. Finally, Fig. 5(b) also shows that the cubic phase C_3A has an unexpected variation of the lattice parameter

Optical Materials EXPRESS

C as a function of x_{Ca}. Since the concentration of the C_3A in the material is small, the relative error in the structural data is larger than for the hexagonal and monoclinic phases. Moreover, we dońt know if there is some interference from the stoichiometry problem mentioned in section 3.2. For these reasons we do not feel we have enough information to explain the result for C_3A presented in Fig. 5(b) at the present time.

Finally, it is necessary to comment on the instability of the $BaAl_2O_4$ lattice under electron bombardment after prolonged shelf life in air at room temperature as presented in Fig, 9(a). It is perhaps fair to assume that the rather wide channels formed by the AlO_4 tetrahedra in $BaAl_2O_4$ allow faster diffusion of O_2, CO_2 and H_2O into the crystal than the channels in the sister materials $CaAl_2O_4$ and $SrAl_2O_4$. Since the shelf life behaviour of the mixed alkaline earth aluminates was not investigated in detail, a more quantitative conclusion cannot be made. It should be noted that only the $BaAl_2O_4$ and $BaMgAl_{10}O_{17}$ (BAM) lattices show oxidation of Eu^{2+} to Eu^{3+} [29,30]. The BAM lattice consists of spinel blocks sandwiched between layers, where the Ba^{2+} (and Eu^{2+}) ions are located. This is in keeping with the large Ba^{2+} cations making the lattices more porous. This also means that the Eu^{2+} cations that are on these sites can easily move off special positions. Indeed the Ba^{2+} cations have excess space on their sites as there is evidence that they can move of their special positions in either hexagonal space group.

Dawson et al. [31] and Boolchand et al. [32] found further evidence for possible movement of the Eu^{2+} cations on cooling in BAM. Dawson et al. based their conclusion on spectroscopy studies, while Boolchand et al. studied BAM by Mössbauer spectroscopy. With this latter technique they found evidence for five different Eu sites: three were for Eu^{2+}, one was for Eu^{3+} and the final one was a mixed valence site [32]. The mixed valence site implies two sites (one an Eu^{2+} and the other an Eu^{3+}) close enough to each other for rapid electron exchange. Heating the BAM to oxidise it led to an increase in the amount of Eu^{3+} present. Depending on the amount of Eu present the oxidation product had up to six Eu sites with an additional Eu^{3+} site. On oxidation of the BAM sample containing 20% Eu total, the Eu^{3+} concentration increased from 3% to 68% (after 12 hours at high temp.) and the mixed valence site fell from 17% to less than 1%. In the oxidation of $BaAl_2O_4$:Eu^{2+} in the electron beam of the TEM, reported in this work, the Eu^{2+} cations that were oxidised to Eu^{3+} were likely to have moved off the special Ba^{2+} positions towards the oxygen atoms of the AlO_4 tetrahedra either before or as a consequence of the oxidation. In the case of the oxidised BAM lattice the Mössbauer parameters of the larger amounts of Eu^{3+} are not the same as that of the small amount of Eu^{3+} present before oxidation.

5. Summary

The crystal structure and the PL of BCA doped with Eu^{2+} have been described herein. The most interesting and surprising result is the odd behaviour of the cell parameters of BCA as a function of the molar fraction of Ca. For the hexagonal phase this behaviour is explained in terms of ferroelectricity, in which the spontaneous polarization is the driving force to inflate the lattice. We have planned follow up research, not only to investigate the implications of this hypothesis on (anti-)ferroelectricity, but also to clarify the differences found in the literature about the radiance of the 430 nm band in $BaAl_2O_4$:Eu^{2+}. From the analyses of the PL spectra it has been concluded herein that the hexagonal phase of $BaAl_2O_4$:Eu^{2+} does not change its structure upon adding Ca, contrasting to the adding of Sr, which causes a change to the paraelectric phase [2].

The difference in oxidation behaviour of $BaAl_2O_4$:Eu^{2+} on the one hand and $CaAl_2O_4$:Eu^{2+} and $SrAl_2O_4$:Eu^{2+} on the other hand after prolonged shelf life (in air at room temperature) has been explained in terms of the size of the AlO_4 channels, being more roomy in $BaAl_2O_4$ than those in $SrAl_2O_4$ and $CaAl_2O_4$ and hence facilitating fast(er) diffusion of O_2 and H_2O into the crystals.

Optical Materials EXPRESS

Appendix

Table 3. Hexagonal BA in $Ba_{0.97-x}Ca_xEu_{0.03}Al_2O_4$

Ca content (mole fraction)	Composition (%)	Unit cell parameters		
		a (Å)	c (Å)	V(Å^3)
0	100	10.4452	8.7884	830.4
0.07	100	10.4408	8.782	829.1
0.17	96.7	10.4264	8.7458	823.4
0.27	77.7	10.408	8.711	817.2
0.37	67.9	10.4108	8.7129	817.8
0.47	57.7	10.4132	8.7163	818.5
0.57	45.8	10.4144	8.718	818.9
0.67	30.6	10.4146	8.7179	818.9
0.77	10.9	10.4198	8.7241	820.3
0.87	0	n. a.	n. a.	n. a.
0.97	0	n. a.	n. a.	n. a.
0*)	n. a.	10.47	8.819	837.2

*) Ref. [6].

Table 4. Monoclinic CA in $Ba_{0.97-x}Ca_xEu_{0.03}Al_2O_4$

Ca content (mole fraction)	Composition (%)	Unit cell parameters				
		a (Å)	b(Å)	c (Å)	β (°)	V(Å^3)
0	0	n. a.	n. a.	n. a.	n. a.	n. a.
0.07	0	n. a.	n. a.	n. a.	n. a.	n. a.
0.17	0	n. a.	n. a.	n. a.	n. a.	n. a.
0.27	20	8.80	8.172	15.18	89.6	1092
0.37	29.6	8.7968	8.1806	15.1935	89.691	1093.3
0.47	39.6	8.7612	8.1835	15.2613	90.074	1094.2
0.57	50.5	8.7593	8.1834	15.263	90.062	1094.1
0.67	63.6	8.7581	8.1836	15.2641	90.062	1094
0.77	83.9	8.7574	8.1819	15.2633	90.058	1093.6
0.87	91.1	8.7382	8.1509	15.2407	90.095	1085.5
0.97	92.9	8.6778	8.0976	15.2088	90.128	1071.1
1.00*)	n.a.	8.7	8.092	15.191	90.28	1069.4

*) Ref. [10].

Optical Materials EXPRESS

Table 5. Cubic C_3A (tri-calcium aluminate) in $Ba_{0.97-x}Ca_xEu_{0.03}Al_2O_4$

Ca content (mole fraction)	Composition (%)	Unit cell parameters	
		a (Å)	V (Å^3)
0	0	n. a.	n. a.
0.07	0	n. a.	n. a.
0.17	3.3	15.21	3518
0.27	2.8 (18)	15.22 (2)	3525 (3)
0.37	2.5	15.23	3533
0.47	2.7	15.23	3535
0.57	3.8	15.25	3546
0.67	5.8	15.25	3545
0.77	5.2	15.26	3550
0.87	8.5	15.25	3546
0.97	3.2	15.24	3539
1.00*)	n. a.	15.263	3556

*) Ref. [11].

Table 6. Cubic $C_{12}A_7$ (mayenite) in $Ba_{0.97-x}Ca_xEu_{0.03}Al_2O_4$

Ca content (mole fraction)	Composition (%)	Unit cell parameters	
		a (Å)	V (Å^3)
0.77	0	n.a.	n.a.
0.87	0.41	11.976	1717.5
0.97	3.9	11.983	1720.6
1.00*)	n. a.	11.9794	1719.1

*) Ref. [12].

Funding

Engineering and Physical Sciences Research Council (CONVERTED (JeS no. TS/1003053/1), FAB3D, PRISM (EP/N508974/1), PURPOSE (TP11/MFE/6/1/AA129F; EP-SRC TS/G000271/1)); TECHNOLOGY STRATEGY BOARD (CONVERT).

Acknowledgments

We are grateful to the EPSRC and Technology Strategy Board (TSB) for funding the PURPOSE (TP11/MFE/6/1/AA129F; EP-SRC TS/G000271/1) and CONVERTED (JeS no. TS/1003053/1), PRISM (EP/N508974/1) and FAB3D programs. We are finally grateful to the TSB for funding the CONVERT program.

References

1. L. Yu, D. den Engelsen, J. Gorobez, G. R. Fern, T. G. Ireland, C. Frampton, and J. Silver, "Crystal structure, photoluminescence and cathodoluminescence of $Sr_{1-x}Ca_xAl_2O_4$ doped with Eu^{2+}," Opt. Mater. Express **9**(5), 2175–2195 (2019).
2. M. Volhard, L. Yu, D. den Engelsen, G. Fern, T. Ireland, and J. Silver, "Crystal structure, photoluminescence and cathodoluminescence of $Sr_{1-x}Ba_xAl_2O_4$ doped with Eu^{2+}," *Opt. Mater. Express*, in press.
3. A. Shukla, *Development of a critically evaluated thermodynamic database for the systems containing alkaline-earth oxides*, Thesis, University of Montreal, July 2012.
4. P. Ptáček, *Strontium Aluminate - Cement Fundamentals, Manufacturing, Hydration, Setting Behaviour and Application* (InTech, 2014), Chapter 1.
5. R. C. Ropp, *Encyclopedia of the Alkaline Earth Compounds* (Elsevier, 2013), Chapter 6.

Optical Materials EXPRESS

6. W. Hörkner and H. K. Müller-Buschbaum, "Zur Kristallstruktur von $BaAl_2O_4$," Z. Anorg. Allg. Chem. **451**(1), 40–44 (1979).
7. S. Y. Huang, R. Von Der Mühll, J. Ravez, and M. Couzi, "Phase transition and symmetry in $BaAl_2O_4$," Ferroelectrics **159**(1), 127–132 (1994).
8. A. M. Abakumov, O. I. Lebedev, L. Nistor, G. Van Tendeloo, and S. Amelinkx, "The ferroelectric phase transition in tridymite type $BaAl_2O_4$ studied by electron microscopy," Phase Transitions **71**(2), 143–160 (2000).
9. S. H. Ju, U. S. Oh, J. C. Choi, H. L. Park, T. W. Kim, and C. D. Kim, "Tunable color emission and solid solubility limit in $Ba_{1-x}Ca_xAl_2O_4:Eu_{0.001}{}^{2+}$ phosphors through the mixed states of $CaAl_2O_4$ and $BaAl_2O_4$," Mater. Res. Bull. **35**(11), 1831–1835 (2000).
10. W. Hörkner and H. Müller-Buschbaum, "Zur Kristallstruktur von $CaAl_2O_4$," J. Inorg. Nucl. Chem. **38**(5), 983–984 (1976).
11. P. Mondal and J. W. Jeffery, "The Crystal Structure of Tricalcium Aluminate, $Ca_3Al_2O_6$," Acta Crystallogr., Sect. B: Struct. Crystallogr. Cryst. Chem. **31**(3), 689–697 (1975).
12. H. Boysen, M. Lerch, A. Stys, and A. Senyshyn, "Structure and oxygen mobility in mayenite ($Ca_{12}Al_{14}O_{33}$): a high-temperature neutron powder diffraction study," Acta Crystallogr., Sect. B: Struct. Sci. **63**(5), 675–682 (2007).
13. U. Rodehorst, M. A. Carpenter, S. Marion, and C. M. Henderson, "Structural phase transitions and mixing behaviour of the Ba-aluminate ($BaAl_2O_4$)-Sr-aluminate ($SrAl_2O_4$) solid solution," Mineral. Mag. **67**(5), 989–1013 (2003).
14. J. Ueda, T. Shinoda, and S. Tanabe, "Evidence of three different Eu^{2+} sites and their luminescence quenching processes in $CaAl_2O_4:Eu^{2+}$," Opt. Mater. **41**, 84–89 (2015).
15. G. Blasse and A. Bril, "Fluorescence of Eu^{2+}-activated alkaline-earth aluminates," Philips Res. Rep. **23**, 201–206 (1968).
16. S. H. M. Poort, W. P. Blokpoel, and G. Blasse, "Luminescence of Eu^{2+} in Barium and Strontium Aluminate and Gallate," Chem. Mater. **7**(8), 1547–1551 (1995).
17. B. M. Mothudi, O. M. Ntwaeaborwa, J. R. Botha, and H. C. Swart, "Photoluminescence and phosphorescence properties of MAl2O4:Eu2+, Dy3+ (M = Ca, Ba, Sr) phosphors prepared at an initiating combustion temperature of 500(C)," Phys. B **404**(22), 4440–4444 (2009).
18. B. P. Kore, N. S. Doble, and S. J. Doble, "Study of anomalous emission and irradiation effect on the thermoluminescence properties of barium aluminate," J. Lumin. **150**, 59–67 (2014).
19. R. Stefani, L. C. V. Rodrigues, C. A. A. Carvalho, M. C. F. C. Felinto, H. F. Brito, M. Lastusaari, and J. Hölsä, "Persistent luminescence of Eu^{2+} and Dy^{3+} doped barium aluminate ($BaAl_2O_4:Eu^{2+},Dy^{3+}$) materials," Opt. Mater. **31**(12), 1815–1818 (2009).
20. Q. He, G. Qiu, X. Xu, J. Qiu, and X. Yu, "Photostimulated luminescence properties of Eu^{2+}-doped barium aluminate phosphor," Lumin. **30**(2), 235–239 (2015).
21. M. Peng and G. Hong, "Reduction of Eu^{3+} to Eu^{2+} in $BaAl_2O_4$ phosphor prepared in an oxidizing atmosphere and luminescent properties of $BaAl_2O_4$:Eu," J. Lumin. **127**(2), 735–740 (2007).
22. F. C. Palilla, A. K. Levine, and M. R. Tomkus, "Fluorescent Properties of Alkaline Earth Aluminates of the Type MAl_2O_4 Activated by Divalent Europium," J. Electrochem. Soc. **115**(6), 642–644 (1968).
23. D. den Engelsen, P. G. Harris, T. G. Ireland, G. Fern, and J. Silver, "Symmetry-Related Transitions in the Photoluminescence and Cathodoluminescence Spectra of Nanosized Cubic $Y_2O_3:Tb^{3+}$," ECS J. Solid State Sci. Technol. **4**(12), R145–R152 (2015).
24. D. den Engelsen, P. G. Harris, T. G. Ireland, G. Fern, and J. Silver, "Symmetry-Related Transitions in the Spectrum of Nanosized Cubic $Y_2O_3:Tb^{3+}$," ECS J. Solid State Sci. Technol. **4**(7), R105–R113 (2015).
25. S. Kawaguchi, Y. Ishii, E. Tanaka, H. Tsukasaki, Y. Kubota, and S. Mori, "Giant thermal vibrations in the framework compounds Ba1−xSrxAl2O4," Phys. Rev. B **94**(5), 054117 (2016).
26. M. V. dos S. Rezende, A. B. Andrade, M. E. G. Valerio, and P. J. R. Montes, "The effect of the host composition on the lifetime decay properties of barium/strontium aluminates compounds," J. Appl. Phys. **115**(10), 103510 (2014).
27. S. Y. Huang, R. Von Der Mühll, J. Ravez, J. P. Chaminade, P. Hagenmuller, and M. Couzi, "A propos de la ferroélectricité dans $BaAl_2O_4$," J. Solid State Chem. **109**(1), 97–105 (1994).
28. C. Kittel, "*Introduction to Solid State Physics*", 4th Ed (J. Wiley Inc., 1971), p483.
29. G. Bizarri and B. Moine, "On $BaMgAl_{10}O_{17}:Eu^{2+}$ phosphor degradation mechanism: thermal treatment effects," J. Lumin. **113**(3-4), 199–213 (2005).
30. T. Onimaru, S. Fukuta, T. Misawa, K. Sakita, and K. Betsui, "Study of the effect of water on thermal and operating degradation of $BaMgAl_{10}O_{17}:Eu^{2+}$ (BAM) blue phosphor," J. Soc. Inf. Disp. **13**(1), 45–50 (2005).
31. B. Dawson, M. Ferguson, G. Marking, and A. L. Diaz, "Mechanisms of VUV Damage in $BaMgAl_{10}O_{17}:Eu^{2+}$," Chem. Mater. **16**(25), 5311–5317 (2004).
32. P. Boolchand, K. C. Mishra, M. Raukas, A. Ellens, and P. C. Schmidt, "Occupancy and site distribution of europium in barium magnesium aluminate by ^{151}Eu Mössbauer spectroscopy," Phys. Rev. B **66**(13), 134429 (2002).